1   # Molecular dynamics simulations of structural transformation of

2   # perfluorooctane sulfonate (PFOS) at water/rutile interfaces

3   Guangzhi He*, Meiyi Zhang, Qin Zhou, Gang Pan*

4   Department of Environmental Nano-materials, Research Center for Eco-Environmental Sciences,

5   Chinese Academy of Sciences, Beijing 100085, China.

6   E-mail: gzhhe@rcees.ac.cn, myzhang@rcees.ac.cn, qinzhou@rcees.ac.cn, gpan@rcees.ac.cn

7   *Corresponding author: Guangzhi He (phone: +86-10-62943436; fax: +86-10-62943436; e-mail:

8   gzhhe@rcees.ac.cn); Gang Pan (phone: +86-10-62849686; fax: +86-10-62849686; e-mail:

9   gpan@rcees.ac.cn)

ABSTRACT: Concentration and salinity conditions are the dominant environmental factors affecting the behavior of perfluorinated compounds (PFCs) on the surfaces of a variety of solid matrices (suspended particles, sediments, and natural minerals). However, the mechanism has not yet been examined at molecular scales. Here, the structural transformation of perfluorooctane sulfonate (PFOS) at water/rutile interfaces induced by changes of the concentration level of PFOS and salt condition was investigated using molecular dynamics (MD) simulations. At low and intermediate concentrations all PFOS molecules directly interacted with the rutile (110) surface mainly by the sulfonate headgroups through electrostatic attraction, yielding a typical monolayer structure. As the concentration of PFOS increased, the molecules aggregated in a complex multi-layered structure, where an irregular assembling configuration was adsorbed on the monolayer structure by the van der Waals interactions between the perfluoroalkyl chains. When adding $CaCl_2$ to the system, the multi-layered structure changed to a monolayer again, indicating that the addition of $CaCl_2$ enhanced the critical concentration value to yield PFOS multilayer assemblies. The divalent Ca^{2+} substituted for monovalent K^+ as the bridging counterion in PFOS adsorption. MD simulation may trigger wide applications in study of perfluorinated compounds (PFCs) from atomic/molecular scale.

1. Introduction

Perfluorinated compounds (PFCs) occur globally in water and soil environments (Lau et al., 2007; Route et al., 2014). Perfluorooctane sulfonate (PFOS, $C_8F_{17}SO_3^-$) is the most commonly measured PFCs, and has been included in the list of Stockholm Convention on Persistent Organic Pollutants (POPs) in 2009 as a global contaminant (Wang et al., 2009). Different from other POPs, PFOS has high water solubility. The high persistence and long-range transport of PFOS in environments have prompted increasing concerns regarding its interfacial behavior that is regarded as central to the environmental fate of PFOS and the treatment of high-concentration wastewater (Pan and You, 2010; Xiao et al., 2011; Zhou et al., 2013).

So far, although PFOS has been investigated extensively, little is known about its interfacial microstructure and the interaction that hold PFOS to the surface because it is inaccessible from the existing experimental measurement (Du et al., 2014). However, the microscopic information is essential to enhance our understanding of the environmental fate of PFOS and to develop high performance adsorbents, because the change of assembling structure and interaction may produce a significant impact on its reversibility, lability, and transport in the environment and the efficiency of water treatment. Although the critical micelle concentration (CMC) of PFOS is 4573 mg/L, it is possible to form hemi-micelles on adsorbent surfaces when its concentration reaches the value of 0.01–0.001 of the CMC (Johnson et al., 2007) (a concentration level of PFOS in experiments and water treatment systems). Therefore, increase of PFOS concentrations promotes the nucleation of hemi-micelles and micelles (Yu et al., 2009; Wang and Shih, 2011), which may result in a substantial increase of PFOS at the interface, and a significant change in the macroscopic sorption properties (e.g, the occurrence of multilayer adsorption (Zhao et al., 2011)). Different types of hemi-micelles and multi-layered structures have been proposed based

52   on macroscopic experiments (Chen et al., 2011; Zhang et al., 2011b; Du et al., 2014). However,

53   these structures need to be identified at molecular scales.

54   PFOS is an anionic surfactant, and hence the ionic strength and cation type in solutions are

55   critical in the adsorption of PFOS on solid surfaces (Jeon et al., 2010; You et al., 2010; Wang

56   and Shih, 2011). Different types of cations may yield very different effects on both interaction

57   strength and structure. However, most sorption experiments provide only macroscopic

58   information (e.g., sorption capacity and sorption kinetics) about the interfacial behavior of PFOS,

59   but little insight into the interaction and microstructure. In fact, changes in the sorption isotherms

60   driven by concentration and salinity conditions depend on the interactions between hydrophobic

61   tails, repulsions between headgroups and interactions between surfactant molecules with the

62   solid surface (Yu et al., 2009; Wang and Shih, 2011). These mechanisms are required to be

63   verified by using atomic-molecular level technologies.

64   Molecular dynamics (MD) simulation, which solves the movement of atoms and molecules,

65   provides detailed insights pertaining to structure, energetics, and dynamics of complex

66   multiphase systems. MD simulation has been successfully used to investigate the interfacial

67   behavior of alkyl surfactants, such as sodium dodecyl sulfate (SDS) and n-alkyl polyethylene

68   oxide (Srinivas et al., 2006; Tummala and Striolo, 2008; Dominguez, 2011; Lin et al., 2011;

69   Nunez-Rojas and Dominguez, 2011). Compared with alkyl surfactants, the perfluoroalkyl

70   surfactant may present different assembling features due to the super hydrophobicity and

71   counterion-bridging effects. To our knowledge, how the environmental factors such as

72   concentration and salinity affect the structure and behavior of perfluorinated compounds (PFCs)

73   at solid-water interfaces has not yet been investigated at molecular scales.

74   TiO_2 is one of the most common and technologically important metal oxides for modern

75   science and technology, and shows a relatively high affinity to PFOS (Yuan et al., 2001). Rutile

76   TiO_2 was chosen as the model oxide surface in this MD study. This study is expected to provide

77   an effective way to investigate the microstructures and interaction properties of PFOS at water-

78   metal oxide (e.g., Fe-, Al-, Mn-, and Ti-oxides) interfaces, and may trigger wide applications of

79   MD simulation in describing the structure and environmental behavior of PFCs as MD technique

80   is improving.

81   Here, the structural transformation and interaction properties of PFOS assembled at the

82   water-rutile interface as a function of concentration and salinity conditions were studied using

83   molecular dynamics (MD) simulation. The surface aggregation was characterized in terms of

84   structure, shape, and associated mode. Effects of salinity on the surface assembling properties of

85   PFOS were investigated by adding $CaCl_2$ to the simulated system. The conformational feature of

86   PFOS was described using the atomic density profile and angle distribution analysis. The role of

87   counterions (K^+, Ca^{2+}) in the formation of surface aggregates was characterized with the radial

88   distribution functions between atoms.

89 **2. Methods**

90   All simulations were carried out using the COMPASS (Condensed-phase Optimized

91   Molecular Potentials for Atomistic Simulation Studies) force field as implemented in the

92   Discover module in Materials Studio package (Accelrys Software Inc.). The functional form of

93   COMPASS force field is given as follows (Sun, 1998; Zhang et al., 2011a):

$$E_{pot} = \sum_b \left[K_2(b-b_0)^2 + K_3(b-b_0)^3 + K_4(b-b_0)^2 \right] \tag{a}$$

$$+ \sum_\theta \left[H_2(\theta-\theta_0)^2 + H_3(\theta-\theta_0)^3 + H_4(\theta-\theta_0)^2 \right] \tag{b}$$

$$+ \sum_\phi \left[V_1\left(1-\cos(\phi-\phi_1^0)\right) + V_2\left(1-\cos(2\phi-\phi_2^0)\right) + V_3\left(1-\cos(3\phi-\phi_3^0)\right) \right] \tag{c}$$

$$+ \sum_\chi K_\chi(\chi-\chi_0)^2 \tag{d}$$

$$+ \sum_b \sum_{b'} F_{bb'}(b-b_0)(b'-b_0') \tag{e}$$

$$+ \sum_\theta \sum_{\theta'} F_{\theta\theta'}(\theta-\theta_0)(\theta'-\theta_0') \tag{f}$$

$$+ \sum_b \sum_\theta F_{b\theta}(b-b_0)(\theta-\theta_0) \tag{g}$$

$$+ \sum_b \sum_\phi (b-b_0)(V_1\cos\phi + V_2\cos 2\phi + V_3\cos 3\phi) \tag{h}$$

$$+ \sum_b \sum_\phi (b'-b_0')(V_1\cos\phi + V_2\cos 2\phi + V_3\cos 3\phi) \tag{i}$$

$$+ \sum_\theta \sum_\phi (\theta-\theta_0)(V_1\cos\phi + V_2\cos 2\phi + V_3\cos 3\phi) \tag{j}$$

$$+ \sum_\phi \sum_\theta \sum_{\theta'} K_{\phi\theta\theta'}\cos\phi(\theta-\theta_0)(\theta'-\theta_0') \tag{k}$$

$$+ \sum_{i>j} \frac{q_i q_j}{\varepsilon r_{ij}} \tag{l}$$

$$+ \sum_{i>j} \left[\frac{A_{ij}}{r_{ij}^9} - \frac{B_{ij}}{r_{ij}^6} \right] \tag{m}$$

94

95   The total potential energy (E_{pot}) contains the bond stretching (a), angle bending (b), torsion

96   (c), out of plane coordinate (d), cross-coupling (e) to (k), Coulombic interaction (l), and van der

97   Waals interaction (m) terms. K, H, F, and V are force-field parameters. The b, θ, ϕ, and χ

98   represent bond length, bending angle, torsion angle, and out-of-plane angle, respectively. The

99   parameters b_0, θ_0, ϕ_0, and χ_0 are the ideal values at zero energy. COMPASS has proven to be

100   suitable for simulating titanium oxides (Kornherr et al., 2004; Kornherr et al., 2006; Zhang et al.,

101   2011a), surfactants (Ryjkina et al., 2002), and perfluorinated compounds (Prathab et al., 2006; Li

102   et al., 2013). The agreement between our calculated PFOS structure and the DFT-calculated

6

103 results (see Supplementary data) indicated that the COMPASS force field is reliable for the

104 description of PFOS. Partial atomic charges used in COMPASS are presented in Table 1.

105   The (110) crystal plane was used as the surface because it is the predominantly exposed

106 plane of natural rutile (60%) (Perron et al., 2007). The dimensions of the solid model were

107 $4.1 \times 3.9 \times 1.3$ nm^3, which contained 766 TiO$_2$ molecules. The initial configuration of the

108 interfacial system was prepared from a monolayer of PFOS molecules (a sulfonate headgroup

109 attached to eight perfluorinated carbon atoms with a length of ~1.0 nm) with the sulfonate

110 headgroups pointed to the surface (~8 Å above the substrate). The initial structure of PFOS is

111 shown in Table 2. K$^+$ ions were added close to the headgroups to neutralize the charge of anionic

112 PFOS (i.e., the potassium salt of PFOS). To reach a water density of ~1.0 g/cc within the

113 solution layer of $4 \times 4 \times 4$ nm^3, 2000 water molecules were used to simulate the solvent

114 environment. The water was simulated using the simple point charge (SPC) model (Berendsen et

115 al., 1987), which worked reliably with the COMPASS force field. The atoms in rutile were

116 constrained to their equilibrium bulk positions, while the structures of PFOS and water

117 molecules were optimized during the simulations (Li and Choi, 2007; Prathab et al., 2007;

118 Nunez-Rojas and Dominguez, 2011). Periodic boundary conditions were imposed, and these

119 systems were separated from their periodic images by a vacuum gap of 6 nm to eliminate

120 spurious interactions between the periodic replicas in the Z direction (Dominguez, 2009; Monti

121 et al., 2012). The resulted final box was approximately $4 \times 4 \times 12$ nm^3.

122   The simulation was performed under three different PFOS concentrations (25, 36, and 64

123 PFOS molecules) to investigate how the concentration levels affected the interfacial assembling

124 behavior of PFOS. In order to explore the salinity effects, a certain number of Ca^{2+} and Cl$^-$ were

125 added to the systems to achieve a ratio of PFOS to CaCl$_2$ being 1:1. The systems were first

126 energetically minimized for 5000 steps using the smart minimizer method, which switches from

127 steepest-descent to conjugated gradient method as the energy derivatives decrease to accelerate

128 the computation. After the initialization, all the MD simulations were conducted in the canonical

129 ensemble (NVT) at a constant temperature of 298 K maintained using Andersen thermostat

130 (Andersen, 1980). The equations of motion were integrated with the velocity Verlet algorithm

131 with a time step of 1 fs (Verlet, 1967). The electrostatic interactions were treated using the Ewald

132 method (Plimpton, 1995), and the Van der Waals interactions were handled with atom-based

133 summation method using a cutoff distance of 9.5 Å with long-range corrections added. The

134 simulations were confirmed to have reached equilibrium within 15 ns by monitoring the structure

135 and shape of PFOS aggregates as a function of time. Therefore, all the systems were finally

136 equilibrated for 18 ns.

137 The selection of parameters and models was justified by performing test calculations (see

138 Supplementary data). Increasing the orbital cutoff from 9.5 to 12.0 Å had no obvious effect on

139 the interfacial structure and properties of PFOS. Similarly, no obvious change was found in the

140 equilibrium structure when we started the simulation with a different initial configuration (i.e.,

141 the PFOS molecules parallel to the surface), indicating that the MD results do not depend on the

142 initial conditions. These tests verified that the present computational settings and models were

143 reliable for describing the structure and properties of PFOS at water-rutile interface.

144 **3. Results and discussion**

145 *3.1. Concentration effects*

146 The equilibrium structures of PFOS assembled at the water-rutile interface under three

147 different (low, intermediate, and high) concentration conditions are present in Fig. 1. A structural

148 transformation driven by an increment of PFOS concentration was clearly identified. At the low

149 and intermediate concentrations, all PFOS molecules directly interacted with the rutile (110)

150 surface mainly by the sulfonate headgroups through electrostatic attraction, and well arrayed in a

151 monolayer (Fig. 1a-b). It was observed that the sulfonate headgroups close to the solid surfaces

152 were linked together by the K^+ ions, leaving the perfluoroalkyl tails away from the surface. As

153 the concentration increased, PFOS molecules arrayed in a different pattern, where a number of

154 PFOS molecules were adsorbed on the monolayer structure by the van der Waals interactions

155 between the perfluoroalkyl chains, forming a multilayer aggregate (Fig. 1c).

156   The PFOS-surface interaction was depicted from the density profiles of the O atoms of the

157 sulfonate headgroups in the Z-direction (i.e. normal to the solid surfaces, Fig. 2a). The

158 orientation of PFOS molecules at the water-rutile interface was determined by the angle (θ)

159 between the C1-C8 vector (C1 is the C atom attached to the sulfonate headgroup, and C8 is the C

160 atom at the end of the perfluoroalkyl chain) and the surface normal (Fig. 2b). The density

161 profiles showed that the sulfonate headgroups interacted with the rutile surfaces mainly at the

162 distance of 2.0–3.5 Å (see the main peaks in Fig. 2a). At low and intermediate concentrations,

163 more than 85% of PFOS molecules were located on the surface with the angle θ less than 45°

164 (Fig. 2b), indicating that most of the PFOS preferred to align perpendicular to the substrate. This

165 conformation is favorable for the electrostatic interaction between the sulfonate headgroups and

166 the solid surface. At high concentration the second adsorbed layer was observed, corresponded to

167 the peaks of the sulfonate headgroups at 17.5-25.0 Å in Fig. 2a. In the second layer, the PFOS

168 molecules were inclined to the surface with an angle range from 0° to 90° (Fig. 2b) and hence

169 formed an irregular assembling configuration (Fig. 1c).

170 *3.2. Salinity effects*

171　　　　When Ca^{2+} ions were added to the system, PFOS displayed a different assembling behavior

172　in terms of the morphology and layer formation (Fig. 3 and Fig. 4a). The angles θ became

173　smaller as the PFOS concentration increased (Fig. 4b), indicating that the PFOS monolayer

174　underwent an ordering transformation. When Ca^{2+} was present, PFOS molecules were inclined to

175　the surface with an angle range from 0° to 80° and formed a relatively irregular monolayer

176　structure at the low concentration, whereas arrayed in a well-ordered monolayer pattern with the

177　perfluoroalkyl chains nearly perpendicular to the substrate (all the angles θ less than 30°) under

178　the high concentration condition. At high PFOS concentration, the multi-layered structure (Fig.

179　1c) changed to a monolayer again when adding $CaCl_2$ (Fig. 3c), indicating that the addition of

180　$CaCl_2$ enhanced the critical concentration value for the occurrence of PFOS multilayer

181　adsorption.

182　*3.3. Counterion-bridging effects*

183　　　　To identify the role of the counterions (K^+ and Ca^{2+}) in the interfacial processes of PFOS,

184　the K-O(3) and Ca-O(3) [O(3), the O atoms on the -SO_3 headgroups] radial distribution functions

185　(RDFs) were analyzed (Fig. 5a and c). An enlarged snapshot of PFOS interacted with K^+ and

186　Ca^{2+} are present in Fig. 5b and d, which provided an atomic picture for counterion-bridging

187　mechanism in PFOS adsorption. As shown in Fig. 5b, the K^+ associated with the sulfonate

188　headgroups of PFOS molecules at the surfaces, reducing the lateral repulsive force between the

189　anionic sulfonate groups and instead inducing an effective attraction. When $CaCl_2$ was added to

190　the system, the divalent Ca^{2+} substituted for monovalent K^+ as the bridging counterion (Fig. 5d).

191　The RDFs were dominated by two peaks at ~2.3 and ~4.3 Å for PFOS-K^+ interaction while at

192　~2.0 and ~4.1 Å for PFOS-Ca^{2+} interaction (Fig. 5a and c), which corresponded to the distances

193　between the K^+/Ca^{2+} and the neighbor and non-neighbor O atoms of two adjacent sulfonate

194 groups (Fig. 5b and d). These results of RDFs indicated that the salinity conditions imposed a

195 difference towards the surface aggregation of PFOS, and the highly charged Ca^{2+} led to stronger

196 interaction with the sulfonate groups.

197 **4. Conclusions**

198   The molecular dynamics (MD) results indicated that concentration and salinity conditions

199 significantly affected the assembling behavior of PFOS at the solid-water interface. At low and

200 intermediate concentrations, PFOS molecules directly interacted with the rutile surface mainly

201 by the sulfonate headgroups through electrostatic attraction, and aggregated in a regular

202 monolayer structure. As the concentration increased, PFOS molecules arrayed in a different

203 pattern, where an irregular assembling configuration was adsorbed on the monolayer structure by

204 the van der Waals interactions between the perfluoroalkyl chains, forming a multilayer

205 aggregate. When adding $CaCl_2$ to the system, the multi-layered structure changed to a monolayer

206 again, indicating that the addition of $CaCl_2$ enhanced the critical concentration value for the

207 occurrence of PFOS multilayer adsorption. An atomic picture for the counterion-bridging in

208 PFOS adsorption was provided, where the highly charged Ca^{2+} substituted for K^+ as the bridging

209 ion to link the sulfonate groups and thus caused the occurrence of surface aggregation. MD

210 simulation provides new perspective for the sorptive characteristics of PFOS, and may trigger

211 wide applications in study of perfluorinated compounds (PFCs) from atomic/molecular scale.

216 **Appendix A. Supplementary data**

217   The validation of computational settings and models. Supplementary data associated with

218 this article can be found in the online version, at

219 **References**

220 Andersen, H.C., 1980. Molecular dynamics simulations at constant pressure and/or temperature.
221 J. Chem. Phys. 72, 2384-2393.

222 Berendsen, H.J.C., Grigera, J.R., Straatsma, T.P., 1987. The missing term in effective pair
223 potentials. J. Phys. Chem. 91, 6269-6271.

224 Chen, X., Xia, X., Wang, X., Qiao, J., Chen, H., 2011. A comparative study on sorption of
225 perfluorooctane sulfonate (PFOS) by chars, ash and carbon nanotubes. Chemosphere 83, 1313-
226 1319.

227 Dominguez, H., 2009. Structure of the sodium dodecyl sulfate surfactant on a solid surface in
228 different NaCl solutions. Langmuir 25, 9006-9011.

229 Dominguez, H., 2011. Structural transition of the sodium dodecyl sulfate (SDS) surfactant
230 induced by changes in surfactant concentrations. J. Phys. Chem. B 115, 12422-12428.

231 Du, Z., Deng, S., Bei, Y., Huang, Q., Wang, B., Huang, J., Yu, G., 2014. Adsorption behavior
232 and mechanism of perfluorinated compounds on various adsorbents-a review. J. Hazard. Mater.
233 274, 443-454.

234 Jeon, J., Kannan, K., Lim, H.K., Moon, H.B., Ra, J.S., Kim, S.D., 2010. Bioaccumulation of
235 perfluorochemicals in Pacific oyster under different salinity gradients. Environ. Sci. Technol. 44,
236 2695-2701.

237 Johnson, R.L., Anschutz, A.J., Smolen, J.M., Simcik, M.F., Penn, R.L., 2007. The adsorption of
238 perfluorooctane sulfonate onto sand, clay, and iron oxide surfaces. J. Chem. Eng. Data 52, 1165-
239 1170.

240 Kornherr, A., Tortschanoff, A., Portuondo-Campa, E., van Mourik, F., Chergui, M., Zifferer, G.,
241 2006. Modelling of aqueous solvation of eosin Y at the rutile $TiO_2(110)$/water interface. Chem.
242 Phys. Lett. 430, 375-379.

243 Kornherr, A., Vogtenhuber, D., Ruckenbauer, M., Podloucky, R., Zifferer, G., 2004. Multilayer
244 adsorption of water at a rutile $TiO_2(110)$ surface: towards a realistic modeling by molecular
245 dynamics. J. Chem. Phys. 121, 3722-3726.

246 Lau, C., Anitole, K., Hodes, C., Lai, D., Pfahles-Hutchens, A., Seed, J., 2007. Perfluoroalkyl
247 acids: a review of monitoring and toxicological findings. Toxicol. Sci. 99, 366-394.

248 Li, C., Choi, P., 2007. Molecular dynamics study of the adsorption behavior of normal alkanes
249 on a relaxed alpha-Al$_2$O$_3$ (0001) surface. J. Phys. Chem. C 111, 1747-1753.

250 Li, Y., Niu, J., Shen, Z., Feng, C., 2013. Size effect of single-walled carbon nanotube on
251 adsorption of perfluorooctanesulfonate. Chemosphere 91, 784-790.

252 Lin, S., Shih, C.-J., Strano, M.S., Blankschtein, D., 2011. Molecular insights into the surface
253 morphology, layering structure, and aggregation kinetics of surfactant-stabilized graphene
254 dispersions. J. Am. Chem. Soc. 133, 12810-12823.

255 Monti, S., van Duin, A.C.T., Kim, S.-Y., Barone, V., 2012. Exploration of the conformational
256 and reactive dynamics of glycine and diglycine on TiO$_2$: computational investigations in the gas
257 phase and in solution. J. Phys. Chem. C 116, 5141-5150.

258 Nunez-Rojas, E., Dominguez, H., 2011. Computational studies on the behavior of sodium
259 dodecyl sulfate (SDS) at TiO$_2$(rutile)/water interfaces. J. Colloid Interface Sci. 364, 417-427.

260 Pan, G., You, C., 2010. Sediment-water distribution of perfluorooctane sulfonate (PFOS) in
261 Yangtze River estuary. Environ. Pollut. 158, 1363-1367.

262 Perron, H., Domain, C., Roques, J., Drot, R., Simoni, E., Catalette, H., 2007. Optimisation of
263 accurate rutile TiO$_2$ (110), (100), (101) and (001) surface models from periodic DFT calculations.
264 Theor. Chem. Acc. 117, 565-574.

265 Plimpton, S., 1995. Fast parallel algorithms for short-range moelcular dynamics. J. Comput.
266 Phys. 117, 1-19.

267 Prathab, B., Aminabhavi, T.M., Parthasarathi, R., Manikandan, P., Subramanian, V., 2006.
268 Molecular modeling and atomistic simulation strategies to determine surface properties of
269 perfluorinated homopolymers and their random copolymers. Polymer 47, 6914-6924.

270 Prathab, B., Subramanian, V., Aminabhavi, T.M., 2007. Molecular dynamics simulations to
271 investigate polymer-polymer and polymer-metal oxide interactions. Polymer 48, 409-416.

272 Route, W.T., Key, R.L., Russell, R.E., Lindstrom, A.B., Strynar, M.J., 2014. Spatial and
273 temporal patterns in concentrations of perfluorinated compounds in bald eagle nestlings in the
274 Upper Midwestern United States. Environ. Sci. Technol. 48, 6653-6660.

275 Ryjkina, E., Kuhn, H., Rehage, H., Muller, F., Peggau, J., 2002. Molecular dynamic computer
276 simulations of phase behavior of non-ionic surfactants. Angew. Chem., Int. Ed. 41, 983-986.

277 Srinivas, G., Nielsen, S.O., Moore, P.B., Klein, M.L., 2006. Molecular dynamics simulations of
278 surfactant self-organization at a solid-liquid interface. J. Am. Chem. Soc. 128, 848-853.

279 Sun, H., 1998. COMPASS: an ab initio force-field optimized for condensed-phase applications -
280 overview with details on alkane and benzene compounds. J. Phys. Chem. B 102, 7338-7364.

281 Torres, F.J., Ochoa-Herrera, V., Blowers, P., Sierra-Alvarez, R., 2009. Ab initio study of the
282 structural, electronic, and thermodynamic properties of linear perfluorooctane sulfonate (PFOS)
283 and its branched isomers. Chemosphere 76, 1143-1149.

284 Tummala, N.R., Striolo, A., 2008. Role of counterion condensation in the self-assembly of SDS
285 surfactants at the water-graphite interface. J. Phys. Chem. B 112, 1987-2000.

286 Verlet, L., 1967. Computer experiments on calssical fluids. 1. Thermodynamical properties of
287 Lennard-Jones moleculles. Phys. Rev. 159, 98-&.

288 Wang, F., Shih, K., 2011. Adsorption of perfluorooctanesulfonate (PFOS) and
289 perfluorooctanoate (PFOA) on alumina: influence of solution pH and cations. Water Res. 45,
290 2925-2930.

291 Wang, T., Wang, Y., Liao, C., Cai, Y., Jiang, G., 2009. Perspectives on the inclusion of
292 perfluorooctane sulfonate into the Stockholm Convention on persistent organic pollutants.
293 Environ. Sci. Technol. 43, 5171-5175.

294 Xiao, F., Zhang, X., Penn, L., Gulliver, J.S., Simcik, M.F., 2011. Effects of monovalent cations
295 on the competitive adsorption of perfluoroalkyl acids by kaolinite: experimental studies and
296 modeling. Environ. Sci. Technol. 45, 10028-10035.

297 You, C., Jia, C., Pan, G., 2010. Effect of salinity and sediment characteristics on the sorption and
298 desorption of perfluorooctane sulfonate at sediment-water interface. Environ. Pollut. 158, 1343-
299 1347.

300 Yu, Q., Zhang, R., Deng, S., Huang, J., Yu, G., 2009. Sorption of perfluorooctane sulfonate and
301 perfluorooctanoate on activated carbons and resin: kinetic and isotherm study. Water Res. 43,
302 1150-1158.

303 Yuan, Q.Z., Ravikrishna, R., Valsaraj, K.T., 2001. Reusable adsorbents for dilute solution
304 separation. 5. Photodegradation of organic compounds on surfactant-modified titania. Sep. Purif.
305 Technol. 24, 309-318.

306 Zhang, H., Lu, X., Leng, Y., Watari, F., Weng, J., Feng, B., Qu, S., 2011a. Effects of aqueous
307 environment and surface defects on Arg-Gly-Asp peptide adsorption on titanium oxide surfaces
308 investigated by molecular dynamics simulation. J. Biomed. Mater. Res., A 96A, 466-476.

309 Zhang, Q., Deng, S., Yu, G., Huang, J., 2011b. Removal of perfluorooctane sulfonate from
310 aqueous solution by crosslinked chitosan beads: sorption kinetics and uptake mechanism.
311 Bioresour. Technol. 102, 2265-2271.

312 Zhao, D., Cheng, J., Vecitis, C.D., Hoffmann, M.R., 2011. Sorption of perfluorochemicals to
313 granular activated carbon in the presence of ultrasound. J. Phys. Chem. A 115, 2250-2257.

314 Zhou, Q., Pan, G., Zhang, J., 2013. Effective sorption of perfluorooctane sulfonate (PFOS) on
315 hexadecyltrimethylammonium bromide immobilized mesoporous SiO_2 hollow sphere.
316 Chemosphere 90, 2461-2466.

317

318

319

320 **Table 1.** Partial atomic charges used to model the assembly of PFOS at the water-rutile interface

Atom	Charges/e
S	1.474
O (in SO_3)	-0.706
C (in $S-CF_2$)	0.166
C (in CF_2-CF_2)	0.520
C (in CF_3)	0.780
F	-0.260
K	1.000
Ti	1.600
O (in TiO_2)	-0.800
O (in H_2O)	-0.820
H	0.410

321 **Table 2.** Initial structure of PFOS molecule*

Distance	Value (Å)	Angle	Value (°)
S-O	1.48	S-C-C	116
S-C	1.91	C-C-C	114
C-C	1.57		
C-F	1.36		

322 *The structural parameters are from the DFT-calculated data in the literature (Torres et al., 2009).
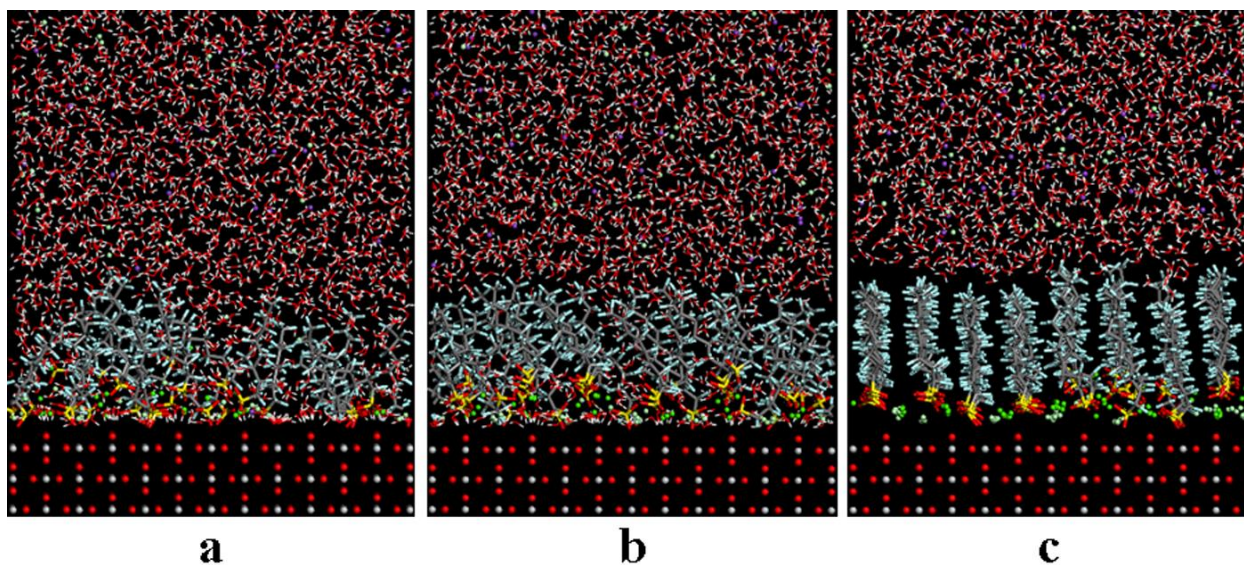
323
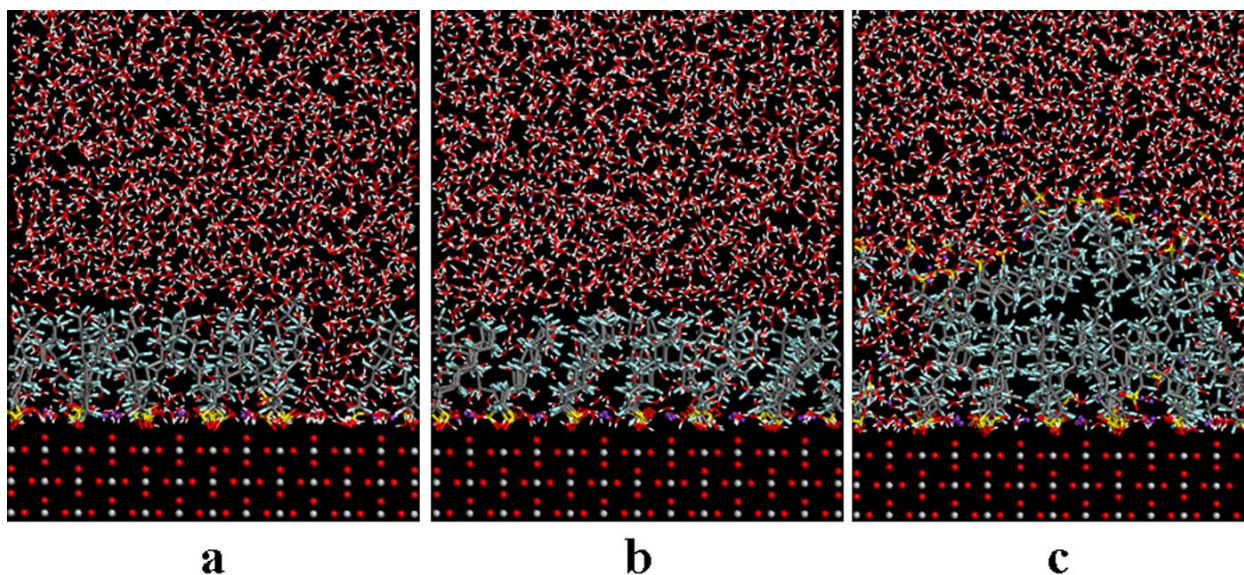
Fig. 1. Snapshot of the final structure of the PFOS aggregates on the rutile (110) surface under three different concentration conditions [(a) low; (b) intermediate; (c) high]. Yellow balls with three surrounding red balls denote the sulfonate headgroups, and the blue-gray sticks denote the C-F chains. The small purple circles represent K^+ ions, and the red-gray lines represent water molecules. For TiO_2, gray and red balls represent Ti and O atoms, respectively.
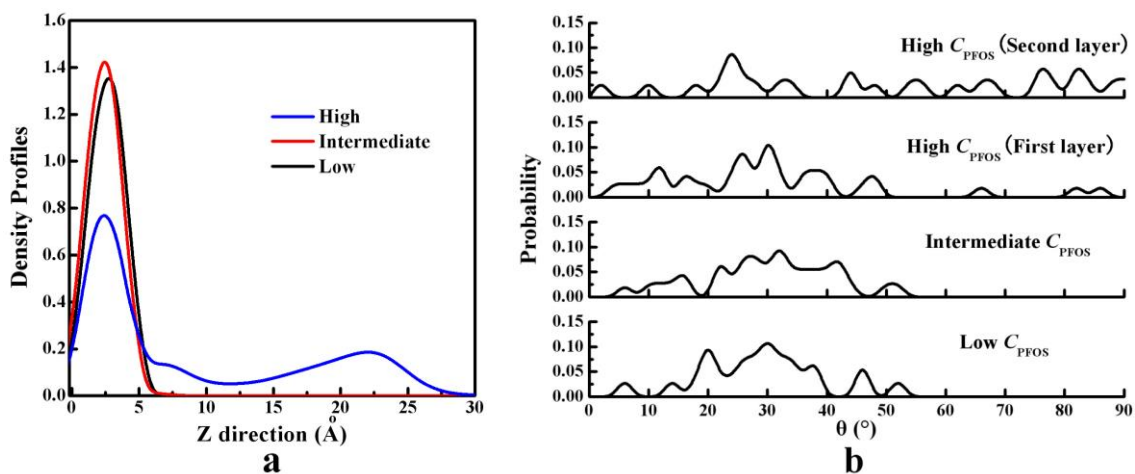

Fig. 2. Conformational feature of PFOS molecules on the rutile (110) surface at three different concentrations: (a) density profiles of the O atoms of the sulfonate headgroups along the Z direction; (b) angle distribution of PFOS with respect to the surface normal.

16

334
335 **Fig. 3.** Snapshot of the final structure of the PFOS aggregates on the rutile (110) surface under

336 three different concentration conditions [(a) low; (b) intermediate; (c) high] with $CaCl_2$ added to

337 the systems. The green circles represent Ca^{2+} ions, and the cyan circles represent Cl^- ions. The

338 color legend of the other atoms is the same as that of Fig. 1.
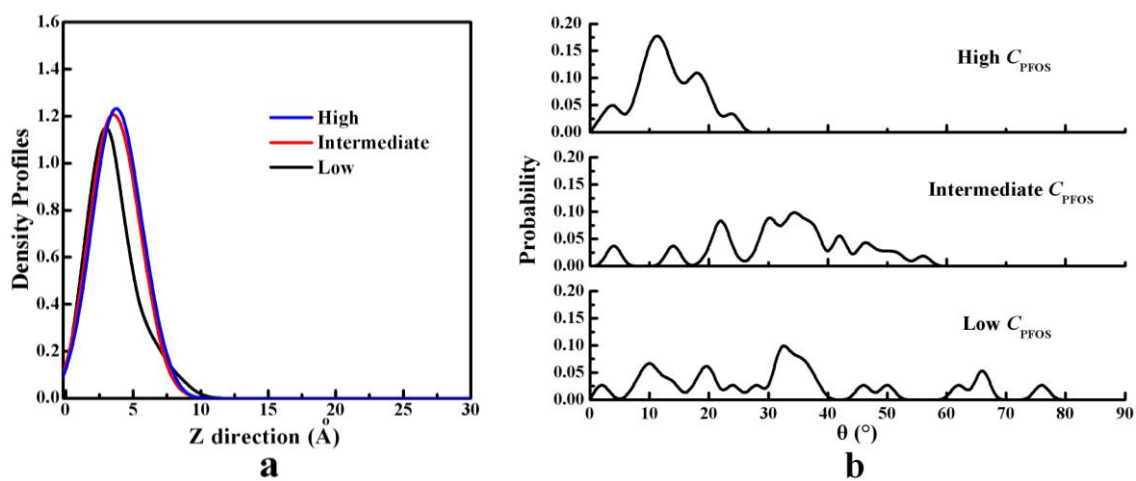
339

340 **Fig. 4.** Conformational feature of PFOS molecules on the rutile (110) surface at three different

341 concentrations with $CaCl_2$ added to the systems: (a) density profiles of the O atoms of the

342 sulfonate headgroups along the Z direction; (b) angle distribution of PFOS with respect to the

343 surface normal.

17

344
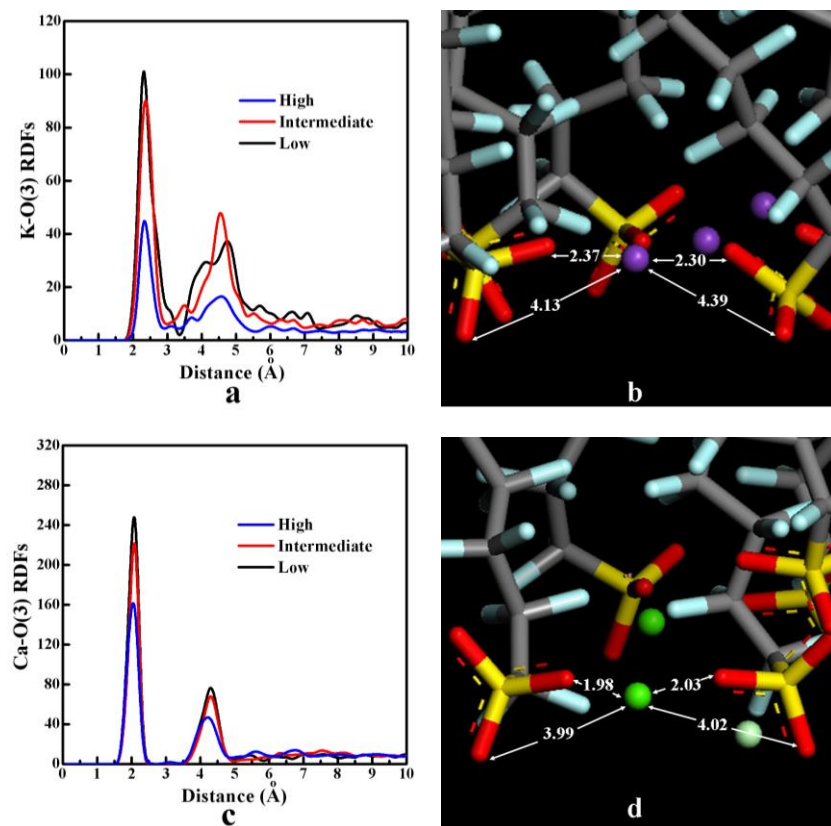
Fig. 5. Counterion bridging in PFOS surface aggregation: (a) K-O(3) RDFs; (b) a snapshot of PFOS-K$^+$ interaction; (c) Ca-O(3) RDFs; (d) a snapshot of PFOS-Ca^{2+} interaction. The color legend is the same as that of Fig. 1 and 3. The distances are shown in angstroms.

18